

Application of IVIM Analysis for Cryoablation Post-Treatment Verification

Shalini Ranmuthu^{1,2}, Joshua Yung¹, Kamran Ahrar³, David Fuentes¹, and R Jason Stafford¹

¹Imaging Physics, The University of Texas M.D. Anderson Cancer Center, Houston, Texas, United States, ²Biomedical Engineering, The University of Texas at Austin, Austin, Texas, United States, ³Interventional Radiology, The University of Texas M.D. Anderson Cancer Center, Houston, Texas, United States

Introduction

Contrast enhanced magnetic resonance imaging (CE-MRI) is often used for post-treatment verification of renal tumor cryoablations. However, some patients are contraindicated for contrast injection and would benefit from an alternative verification method. Intravoxel incoherent motion (IVIM)-MRI creates contrast between perfusing and non-perfusing compartments by repeatedly imaging with magnetic diffusion gradients of varying strength (b-values) [1]. IVIM can thus be used as a fast, reliable approach to quantify tissue perfusion parameters. In this study, we aim to assess the feasibility of IVIM-MRI as an alternate method for differentiating healthy and ablated tissue in tumor cryoablation applications.

Materials and Methods

All analysis was performed on IVIM and dynamic contrast enhanced-MRI images from 3 different renal cryoablation patients, all acquired on a clinical 1.5T whole body MR system (Espree, Siemens, Erlangen, Germany). The post treatment CE-MRI sequence images (TR/TE = 5.98/2.75 ms, slice thickness = 2.5 mm, flip angle = 10°, Pixel Bandwidth = 250 Hz, matrix = 256x192) were manually segmented into enhancing and non-enhancing tissue compartments using Amira (Fig. 1). These CE segmentations were resampled and registered to perfused and unperfused segmentations of the IVIM images (TR/TE = 6039/84 ms, slice thickness = 6 mm, flip angle = 90°, Pixel Bandwidth = 1371 Hz, NEX = 2, matrix = 192x156; b-values = 0, 50, 150, 300, 600 s/mm²) using the ANTsR toolkit [2]. MATLAB scripts were used to fit the bi-exponential and mono-exponential IVIM models (Eq 1,2) to each voxel to create different IVIM parameter maps of the kidney [1,3]. MATLAB (Mathworks, Natick, MA)'s random forest classification algorithms were then applied to the set of different IVIM parameter maps to identify the feature importance of each IVIM parameter as compared to the segmented CE images (ground truth) [4].

Results and Discussion

The bi-exponential model was used to calculate 3 parameter maps (perfusion fraction, diffusion coefficient, and pseudodiffusion coefficient). The mono-exponential model was then used to calculate an ADC map for each combination of 2 b-values (ie. ADC 0/50, ADC 0/100, ADC 50/100, etc), resulting in an additional 10 maps. The random forest results indicate that of the 13 parameter maps analyzed, the ADC map created using the b=0 and b=600 s/mm² IVIM images had the highest feature importance for both patients (Fig. 2). This suggested that the 0/600 s/mm² ADC map correlated best with our ground truth CE images, and was the ideal candidate for an alternative post-treatment verification sequence. Since this verification map requires only 2 different b-values, the post-treatment verification has the potential to be acquired much more quickly, but still retain the capability to differentiate ablated and healthy tissue similar to that of CE-MRI. However, a larger test sample is needed to verify the correlation and overall parameter importance.

References

- [1] Le Bihan D, et al. Radiology, 1988. 168(2): 497–505.
- [2] Avants, B. B., et al. "ANTs, Advanced Normalization Tools." (2010).
- [3] Patel J, et al. JMRI, 2010. 31: 589-600.
- [4] Breiman L, et al. "Random Forests" (2005).

Eq 1:

$$S_b/S_0 = (1 - PF) \exp(-bD) + PF \exp(-bD^*)$$

Eq 2:

$$S_b = S_0 \exp(-bADC)$$

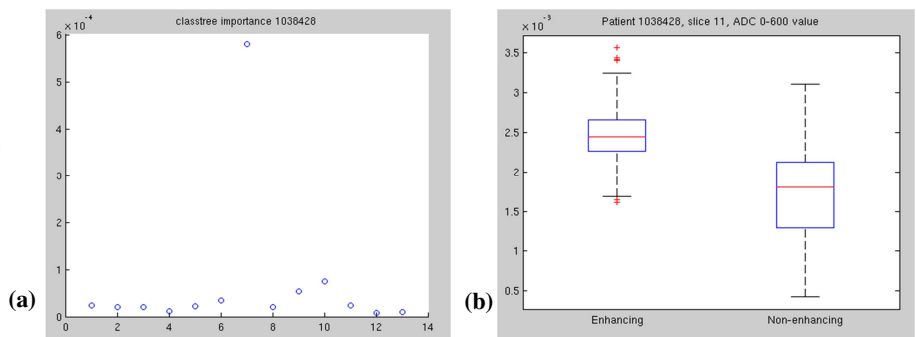


Fig 2: (a) Variable importance graph which demonstrates that ADC 0/600 (parameter 7) has the highest correlation. (b) Boxplots demonstrate a visible difference in the voxels classified as enhancing vs. non-enhancing using ADC 0/600 parameter.

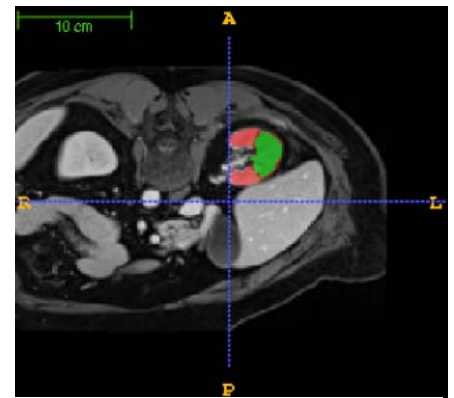


Fig 1: Enhancing and non-enhancing segmentations of CE-MRI images on Amira.